

Variation of Electronic Transitions and Local Structure of $\text{LiNi}_{1/3}\text{Co}_{1/3}\text{Mn}_{1/3}\text{O}_2$ Cathode during Electrochemical Cycling

Beamline

17A X-ray Powder Diffraction beamline
17C Extended X-ray Absorption Fine Structure beamline (EXAFS)

Authors

Y. W. Tsai and B. J. Hwang
National Taiwan University of Science and Technology, Taipei, Taiwan

G. Ceder
Massachusetts Institute of Technology, Cambridge, USA

H. S. Sheu, D. G. Liu, J. F. Lee and B. J. Hwang
National Synchrotron Radiation Research Center, Hsinchu, Taiwan

In-situ X-ray absorption spectroscopic investigations have been carried out to examine the changes of the electronic transitions and local structure at the Mn, Co, and Ni K-edge for the $\text{LiNi}_{1/3}\text{Co}_{1/3}\text{Mn}_{1/3}\text{O}_2$ electrode during charging and discharging process in this study. It was found that only Ni atom in $\text{Li}_{1-x}\text{Ni}_{1/3}\text{Co}_{1/3}\text{Mn}_{1/3}\text{O}_2$ is electroactive from the evolution of the XANES spectra and the bond length variation of Ni-O. The redox pairs of $\text{Ni}^{2+}/\text{Ni}^{3+}$ and $\text{Ni}^{3+}/\text{Ni}^{4+}$ exist and the oxidation states of Mn and Co remain as Mn^{IV} and Co^{III} , respectively, in $\text{Li}_{1-x}\text{Ni}_{1/3}\text{Co}_{1/3}\text{Mn}_{1/3}\text{O}_2$ upon charge and discharge. The oxygen, rather than the transition-metal ions (Ni, Co, and Mn), functions as electron donor at the end of charge. In addition, the irreversible capacity at the first cycle derives mainly from the appearance of inactive Ni, which is evidenced by the energy shift $E - E_0$ of the absorption edge for the Ni absorber and the bond length change of the Ni-O. A decrease/increase of Debye-Waller factor of Ni-O contribution results from a decrease/increase of Jahn-Teller active Ni^{III} concentration during cycling. The trends of the variations for the bond length and Debye-Waller factor for the second shell Mn-M and Ni-M contributions are significant and similar, suggesting the short-range ordering between Ni^{II} and Mn^{IV} may take place in this compound.

Substitution of Ni in $\text{LiNi}_{1-x}\text{Co}_x\text{O}_2$ cathode materials by lower cost materials, such as Mn, is an effective way to improve their initial capacity and cycle life as shown in the work of Tsai et al. This observation led to the development of a series of compounds $\text{LiNi}_x\text{Co}_{1-2x}\text{Mn}_x\text{O}_2$ ($0 \leq x \leq 1/2$) in recent years. Among these classes of compounds the $\text{LiNi}_{1/3}\text{Co}_{1/3}\text{Mn}_{1/3}\text{O}_2$ shows the best cell performance. Hence, it is of interest to investigate the variation of oxidation states and local structure of $\text{LiNi}_{1/3}\text{Co}_{1/3}\text{Mn}_{1/3}\text{O}_2$ upon delithiation and lithiation and X-ray absorption spectroscopy is of particular interest for this purpose. It can provide a fundamental understanding of the charging-discharging mechanism and short-range ordering in the transition-metal-ion layers of the $\text{LiNi}_{1/3}\text{Co}_{1/3}\text{Mn}_{1/3}\text{O}_2$ material.

The systematic changes of the Ni K-edge XANES spectra as a function of x are shown in Fig. 1. The energy positions of the pre-edge peak α and the absorption edge β of the Ni absorber for $\text{Li}_{1-x}\text{Ni}_{1/3}\text{Co}_{1/3}\text{Mn}_{1/3}\text{O}_2$ with $x = 0$ are similar to the reference NiO. Upon delithiation, these peaks shift to higher values and reach absorption

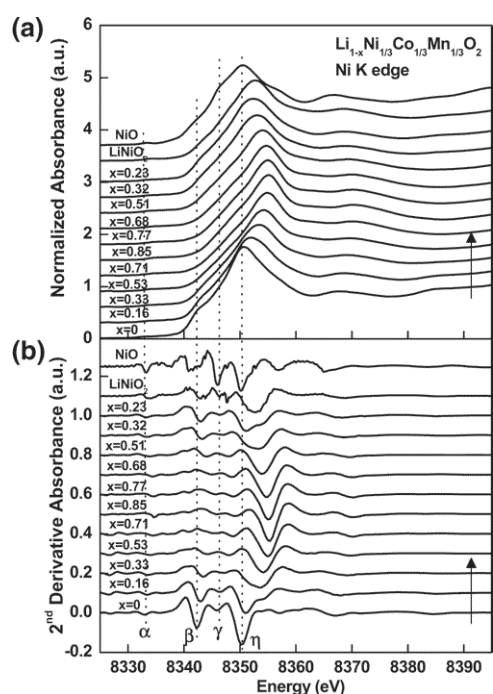


Fig. 1

energies higher than those in LiNiO_2 for $x > 0.85$. The XANES spectra suggest that the redox process is a two-step reaction, $\text{Ni}^{2+}/\text{Ni}^{3+}$ and then $\text{Ni}^{3+}/\text{Ni}^{4+}$. The XANES feature for the Ni K-edge at $x = 0.33$, which agrees well with that of the reference LiNiO_2 , corresponds to a transition state from Ni^{2+} to Ni^{3+} upon charge. Also, the feature is nearly the same at $x = 0.32$ upon discharge. The Ni K-edge XANES results indicate that the irreversible capacity mainly results from a part of Ni^{3+} that cannot be reduced to Ni^{2+} .

The structure parameters of the local environment for the $\text{Li}_{1-x}\text{Ni}_{1/3}\text{Co}_{1/3}\text{Mn}_{1/3}\text{O}_2$ compound obtained by the curve fitting analysis are shown as a function of x in Fig. 2. Figures 2(a)-(f) shows the changes of bond length and Debye-Waller factor for the first shell Mn–O, Co–O, and Ni–O in the $\text{Li}_{1-x}\text{Ni}_{1/3}\text{Co}_{1/3}\text{Mn}_{1/3}\text{O}_2$ compound at different charging and discharging states. At $x = 0$, the bond distances of the Mn–O, Co–O, and Ni–O shells in Fig. 2(a)-(c) are 1.921, 1.929, and 2.045 Å, respectively. It is consistent with their atomic radius, 0.53 Å for Mn^{4+} , 0.545 Å for Co^{3+} , and 0.69 Å for Ni^{2+} . The small values of the Debye-Waller factor for Mn–O, Co–O, and Ni–O are 3.0×10^{-3} , 2.3×10^{-3} , and $3.5 \times 10^{-3} \text{ \AA}^2$, respectively, indicating the absence of Jahn-Teller active Ni^{3+} and Mn^{3+} ions in the pris-

tine material. As the Li ions are deintercalated from at $\text{Li}_{1-x}\text{Ni}_{1/3}\text{Co}_{1/3}\text{Mn}_{1/3}\text{O}_2$ at $x = 1/3$, the bond distances of Mn–O and Co–O decrease only slightly from 1.921 to 1.914 Å and 1.929 to 1.914 Å, respectively, while the bond distance of Ni–O decreases drastically from 2.045 to 1.931 Å, indicating the Ni sites are electroactive. The Debye-Waller factor shows a maximum value of $8.5 \times 10^{-3} \text{ \AA}^2$ for Ni–O in the x range of 0.25 – 0.33, and that for Mn–O and Co–O shows insignificant change in the delithiated process. It suggests that all of the Ni^{2+} ions are oxidized to Jahn-Teller active Ni^{3+} ions and the Mn and Co ions remain in the oxidation states as +4 and +3, respectively. It is further confirmed that the two-step redox reaction of $\text{Ni}^{2+}/\text{Ni}^{3+}$ and $\text{Ni}^{3+}/\text{Ni}^{4+}$ occurs in this compound during one cycle.

The variations of the bond distance and the Debye-Waller factor for the second shell Mn–M, Co–M, and Ni–M contributions are shown in Fig. 3(a)-(f) as a function of x upon charge and discharge. The bond distances in the second shell are similar for Mn–M and Ni–M with values of 2.871 and 2.880 Å, respectively, which is longer than that of 2.858 Å in the second shell Co–M in the pristine $\text{LiNi}_{1/3}\text{Co}_{1/3}\text{Mn}_{1/3}\text{O}_2$ compound. The Debye-Waller factor for the second shell Mn–M and Ni–M varies with the same trend rather than that of the second shell Co–M, which has the maximum values of $4.8 \times 10^{-3} \text{ \AA}^2$ for Mn–M and $6.1 \times 10^{-3} \text{ \AA}^2$ for Ni–M at the x range of 0.5 – 0.6 in $\text{Li}_{1-x}\text{Ni}_{1/3}\text{Co}_{1/3}\text{Mn}_{1/3}\text{O}_2$. Moreover, the changes in the bond length for Mn–M, Co–M, and Ni–M shells are attributed to the variation of bond distance of transition metals on *ab* plane during charging and discharging process. The difference of the bond length between the starting and fully charged states is less in the Co–M shell than in the Mn–M and Ni–M shells. The variations of Debye-Waller factor and bond distance for the second M–M shells observed here provide evidence that the ordering between Ni^{II} and Mn^{IV} takes place in this compound. Because there is no long-range ordering observed in the XRD patterns, we suggest it is short-range ordering between Ni^{II} and Mn^{IV} that can only be observed by the techniques, such as XAS and NMR. Similar phenomena have also been observed in the $\text{LiNi}_{0.65}\text{Co}_{0.25}\text{Mn}_{0.1}\text{O}_2$ compound. A recent computational study combining density functional theory and Monte Carlo simulation shows that the ions arrange

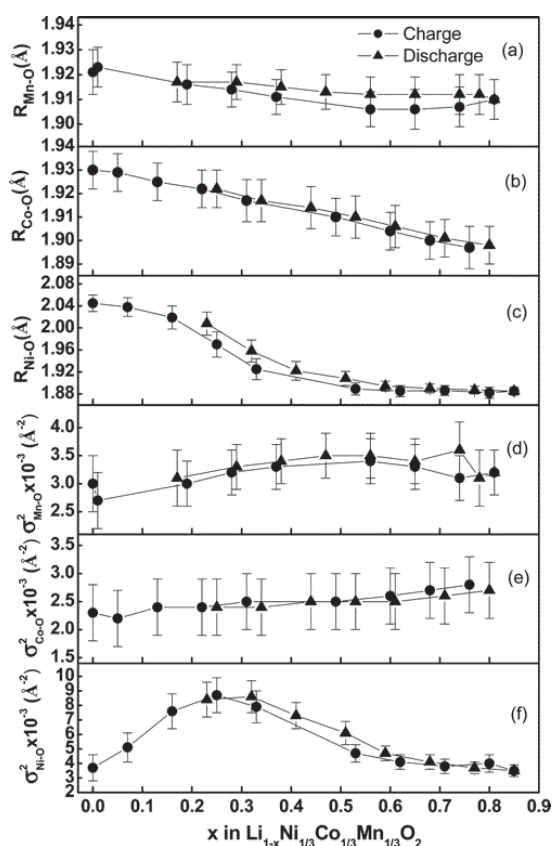
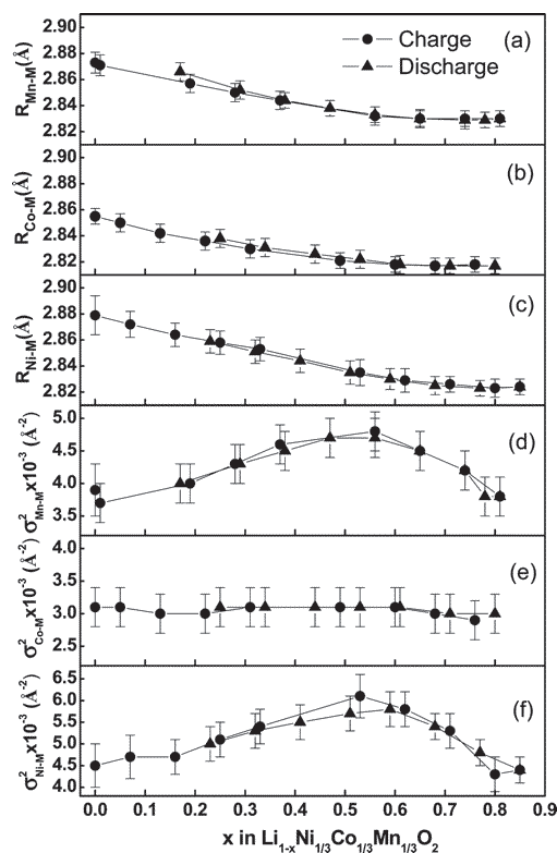


Fig. 2

Fig. 3



in flowerlike patterns with Li surrounded by a hexagon of Mn, which in turn is surrounded by a larger hexagon of Ni, on the layer with composition $\text{Li}_{1/12}\text{Ni}_{5/12}\text{Mn}_{6/12}$ in the $\text{Li}(\text{Ni}_{0.5}\text{Mn}_{0.5})\text{O}_2$ compound. Meanwhile, NMR studies, which provide information about short-range ordering, indicate the Li ions that reside in the transition-metal-ion layer are preferentially surrounded by Mn ions with significantly fewer nearest neighbour Li–Ni bonds than would be expected from a model with random distribution in the $\text{LiNi}_x\text{Mn}_{(2-x)/3}\text{Li}_{(1-2x)/3}\text{O}_2$ compound. Yoon et al have reported that no phase segregation takes place in the $\text{LiNi}_{1/3}\text{Co}_{1/3}\text{Mn}_{1/3}\text{O}_2$ compound from NMR and XANES studies. Although the domain of the short-range order in this compound is probably not significant enough to be observed by NMR and XANES techniques, it can be observed by EXAFS, which is more sensitive to the change of local structure. Therefore, it is suggested that short-range ordering between Ni and Mn ions occurs in this compound but is not as obvious as that in the $\text{LiNi}_x\text{Mn}_{(2-x)/3}\text{Li}_{(1-2x)/3}\text{O}_2$ compound.

The electronic transitions and the local structure of the $\text{Li}_{1-x}\text{Ni}_{1/3}\text{Co}_{1/3}\text{Mn}_{1/3}\text{O}_2$ compound were investigated by in situ X-ray absorption spectroscopy upon

charge and discharge. The XANES data demonstrate the oxidation states for Mn, Co, and Ni absorbers are +4, +3, and +2, respectively, in the pristine $\text{Li}_{1-x}\text{Ni}_{1/3}\text{Co}_{1/3}\text{Mn}_{1/3}\text{O}_2$ compound. During lithiation and delithiation cycle in the potential range of 3 – 4.5 V, an intermediate state of Ni^{3+} is observed from the variation of bond length and the Debye-Waller factor for the M–O shell. A two-step redox reaction involving $\text{Ni}^{2+}/\text{Ni}^{3+}$ and $\text{Ni}^{3+}/\text{Ni}^{4+}$ takes place during cycle, but the oxidation states of Mn and Co remain as Mn^{IV} and Co^{III} , respectively. It suggests that the oxygen, rather than the transition-metal ions (Ni, Co, and Mn), functions as the electron donor at the end of charge. The significant change in the bond length and Debye-Waller factor for the second shell M–M arises mainly from the generation and reduction of the Jahn-Teller active Ni^{III} sites. The trends of the variations for the bond length and Debye-Waller factor for the second shell Mn–M and Ni–M contributions are significant and similar, suggesting the short-range ordering between Ni^{II} and Mn^{IV} may take place in this compound. However, this kind of short-range ordering is probably not significant enough to be observed by NMR.

Experimental Station

X-ray Powder Diffraction end station
X-ray Absorption Spectroscopy end station

Publications

- Y. W. Tsai, B. J. Hwang, G. Ceder, H. S. Sheu, D. G. Liu and J. F. Lee, *Chem. Mater.*, **17**, 3191-99 (2005).
- B. J. Hwang, R. Santhanam, C. H. Chen and Y. W. Tsai, *J. Mater. Chem.* **13**, 1962 (2003).
- D. D. MacNeil, Z. Lu and J. R. Dahn, *J. Electrochem. Soc.* **149**, A1332 (2002).

Contact E-mail

bjh@mail.ntust.edu.tw